Science Advances
AAAS

advances.sciencemag.org/cgi/content/full/4/7/eaar5471/DC1

Supplementary Materials for

Plasticity reveals hidden resistance to extinction under climate change in the global hotspot of salamander diversity

Eric A. Riddell*, Jonathan P. Odom, Jason D. Damm, Michael W. Sears

*Corresponding author. Email: eriddel@clemson.edu

Published 11 July 2018, *Sci. Adv.* **4**, eaar5471 (2018)
DOI: 10.1126/sciadv.aar5471

This PDF file includes:

Supplementary Materials and Methods

Flow-through system design

Water loss and metabolic rates were measured in the laboratory using a flow through system to characterize acclimatization for the field and laboratory experiments. For all experiments, we measured physiological traits of each salamander at night from 1900 to 500 to reduce the influence of circadian rhythms on metabolism. The air was pushed through the flow through system with a sub-sampler pump (SS4; Sable Systems International (SSI); 3840 North Commerce Street, North Las Vegas, NV 89032) at a flow rate of 180 mL/min. After the pump, the air passed through a bubbler bottle to saturate the airstream followed by a dew point generator (DG4; SSI) to control the vapor pressure in the air stream. A flow manifold was used to control the flow rate and divide the airstream for the chambers with the individual salamander. The chambers consisted of acrylic tubes (16 cm x 3.5 cm, volume ~ 153 mL), and salamanders were placed on hardwire mesh inside the chambers to simulate posture while walking on the forest floor and minimize behaviors that reduce water loss rates, such as curling onto oneself. We cycled through individual chambers using a multiplexer (M8; SSI) and subsequently measured the vapor content of the airstream using a RH300 (SSI). The air was scrubbed of water vapor and carbon dioxide using Drierite and soda lime before measuring the flow rate of the air. Drierite was also used daily to baseline the water vapor analyzer. Finally, we measured the oxygen consumption using an Oxzilla (SSI). We used Expedata (SSI) to perform calculations that convert partial pressures of gasses to meaningful physiological values.

Physiological equations

Physiological traits are estimated by converting partial pressures of gases measured from the flow-through system into meaningful physiological values. We measured skin resistance to water loss by converting water vapor pressure (kPa) into water vapor densities using

$$\rho_v = \frac{e}{(T \times R_v)} \quad (1)$$

where T is temperature in Kelvin (K) and R_v is the gas constant for water vapor (461.5 $JK^{-1}kg^{-1}$). The vapor density was then converted to evaporative water loss (EWL; g/s) using the following equation:

$$EWL = \rho_v \times FR \times \frac{1}{60} \quad (2)$$

where FR is the flow rate of the air stream (mL/min) and 1/60 is a conversion factor for mg/min. We then calculated CWL (g $s^{-1}cm^{-2}$) by dividing the rate of water loss by the empirically derived estimates of surface area. We estimated surface area (cm^2) using an equation for the Family Plethodontidae in which surface area = 8.42 x $mass^{0.694}$ (*61*). Finally, calculating the skin resistance to water loss requires appropriate estimation of the boundary layer resistance defined as the resistance to water loss of the microclimate directly surrounding an organism (*51*). By estimating the boundary layer, skin resistance can be calculated using the following equation:

$$r_T = r_i + r_b = \frac{\rho}{CWL} \quad (3)$$

where ρ (g/cm^3) is the vapor density gradient, CWL (g cm^{-2} s^{-1}) is the cutaneous water loss rate, r_i (s/cm) is the skin (or integumentary) resistance, r_b (s/cm) is the boundary layer resistance, and r_T (s/cm) is the total resistance to water loss. For volume of oxygen

consumption, we converted the partial pressure of oxygen to volume of oxygen consumption using:

$$VO_2 = FR_e(F_iO_2 - F"_eO_2)/(1 - F_iO_2) \quad (4)$$

where FR_e is the excurrent flow rate (mL), F_iO_2 is the incurrent fractional concentration of oxygen (20.95%), and $F''O_2$ is the excurrent fractional concentration of oxygen (*62*).

SDM assumptions

We assumed that the seven species within the *P. jordani* complex exhibit the same physiological traits. However, the assumption of similar physiologies is generally appropriate due to their highly conserved climatic niche. We also assumed a lack of geographic variation in plasticity; this assumption seems reasonable given that individuals collected across their elevational gradient exhibited the same capacity to acclimatize. We also assumed that acclimation capacity did not vary with body size, but body size did not influence acclimation capacity in our field based experiment (i.e., no interaction between body size and time period table S1 and S2). As discussed earlier, we also assumed that an individual has immediate access to prey, and they could digest prey immediately. Although unrealistic, these assumptions indicate that our models are conservative in their estimates of extinction. We also lack the spatial resolution to capture fine-scale microhabitat that might buffer salamanders from warming. Salamanders might find suitable microrefugia in stumps and near creek beds; however, a decline in habitat suitability would indicate strict limitations on dispersal, movement, and time available to forage on the surface. Ultimately, these restrictions would have a

highly negative impact on fitness and potentially result in population declines. Finally, we assume that individuals continue to exhibit plasticity in the future.

Thermal performance of $\dot{V}O_2$

In a separate experiment, we measured volume of oxygen consumption ($\dot{V}O_2$) of *P. metcalfi* in the laboratory to estimate energy expenditure for the species range model. We captured these individuals from the same field site in June of 2016 using the same methods as described above. We measured oxygen consumption using the same flow through system as the seasonal measurements of physiology. We used a slower flow rate (100 mL/min) for the metabolic measurements to increase the resolution of the oxygen depletion curves at cool temperatures when metabolic rates are low. The drying power of air was constant across temperature treatments to maintain the same vapor pressure deficits (0.2 kPa or 78% - 94% relative humidity). The experimental temperatures were controlled using incubators (Percival Scientific; I-36VL; 505 Research Drive, Perry IA 50220) which housed the metabolic chambers. Animals were fasted for five days prior to measurements to ensure they were in a post-absorptive state. Prior to the measurement, salamanders acclimated to the experimental temperature for two hours. We measured $\dot{V}O_2$ of 24 individuals in complete darkness from 1900 to 500 at 6˚C, 12˚C, 18˚C, and 24˚C, and each individual was measured three times over a period of 2.5 hr. Each experimental temperature occurred on a single night, and the order of temperature treatments was randomized to avoid potential ordering effects due to acclimation. Statistical models of the thermal performance of $\dot{V}O_2$ were developed using the final measurement recorded for each individual.

Experimental acclimatization of physiology

We assessed acclimatization in *P. metcalfi* by exposing individuals to combinations of temperature and humidity while monitoring changes in skin resistance to water loss (r_i) and volume of oxygen consumption ($\dot{V}O_2$) over a 28-day exposure to temperature and VPD treatments. For the purposes of this study, our primary goal was to establish that individuals exhibit plasticity of the physiological traits of interest. We captured individuals in spring 2016 using the same methods and field site as the previous experiments. We only collected individuals that weighed 3.0 g (+/- 0.5 g) to minimize the influence of body size and age in the study.

Prior to the experiment, salamanders were acclimated to laboratory conditions for one month under cycling thermal conditions controlled by the Percival incubators. The cycling temperatures reflected the conditions that salamanders commonly experience on the forest floor during activity (15˚C) and the temperature that they would experience underground (8.5˚C) during the spring. We based these values on the temperature at the surface and 10 cm below the surface during a typical night of activity in the spring at our field site using the *microclim* dataset (*29*). During the acclimation period, salamanders were provided with moist paper towels and crickets (*Acheta domesitcus*) *ad libitum*. Crickets were no longer provided to the salamanders one week prior to the beginning of the acclimatization study to ensure individuals were in a post-absorptive state. After one week, we measured baseline r_i and $\dot{V}O_2$ of each individual, and individuals were randomly assigned to one of four experimental treatments.

Individuals were randomly assigned to their experimental treatment to test the influence of temperature and humidity on acclimatization. For the cool temperature cycle, salamanders were maintained under the same temperature cycle as the laboratory acclimation period. The warm temperature cycle consisted of temperatures between 22˚C and 16˚C, which reflected the average temperature cycle predicted by our estimates of surface temperature under climate warming. The warm treatment was 7˚C warmer than the cool treatment on average, and the treatments exhibited the same variation in temperature. Temperatures changed continuously in a sinusoidal fashion during the entirety of the experiment. For each temperature cycle, we also tested the influence of humidity on acclimatization by controlling humidity at two different VPDs, 0.25 kPa and 0.5 kPa. These VPDs represent the upper end of the vapor pressure deficits that salamanders experience in nature (see Fig. 1.). We verified these conditions by placing three Hygrochron dataloggers in unoccupied containers in each treatment. The VPDs were controlled by programming the incubators to simultaneously adjust relative humidity as temperatures changed throughout the day to maintain the same VPD. Therefore, we tested acclimatization of physiological traits in response to temperature and VPD treatments using four treatments: (1) warm, wet; (2) warm, dry; (3) cool, wet; (4) cool, dry. However, the purpose of the acclimatization experiment for this study was simply to demonstrate that individuals exhibit physiological plasticity. A more in depth analysis on the effect of treatments occurred in another study (*48*).

We simulated nocturnal activity by moving salamanders from their containers with moist paper towels to containers that simulated the forest floor. We modified the containers for activity by replacing the lid with mesh fabric to facilitate circulation of the

air from the incubator into the container. The bottom of the container consisted of soil to mimic substrate from the field. We exposed salamanders to their conditions for three hours a night for five nights a week. After five nights, we measured physiological traits using a flow-through system (described above) followed by one night of rest. Prior to the measurement, salamanders equilibrated to the experimental temperature for two hours. We measured evaporative water loss and oxygen consumption at a constant temperature of 18˚C and a VPD of 0.5 kPa. We measured physiological traits of each individual five times over a month long period. Each treatment consisted of 30 individuals spread across four shelves; therefore, the acclimatization study consisted of 120 individuals. Each treatment was randomly assigned an incubator at the beginning of the study, and every week, we rotated the individuals and treatment to a new incubator in a random order to reduce any effects of the incubator. Each individual was also assigned to a shelf in the incubator, and each night, we rotated the orientation of the shelf and the order of the shelves to reduce any influence of shelf placement. Therefore, each individual experienced every combination of incubator and shelf at least once during the study.

Environmental data for species distribution model

We estimated thermal and hydric environment for the SDM based upon physical associations with elevation and interactions between temperature and humidity. We calculated fine scale variation in temperature across the southern Appalachian Mountains by correcting for the effect of elevation using the adiabatic lapse rate:

$$T_{final} = T_{initial} - (5.5°C / km) \times \Delta z \quad (5)$$

where Δz is the difference in elevation, $T_{initial}$ is the average temperature, and T_{final} is the calculated temperature (*63*). The value of the adiabatic correction is based upon empirical values for the southern Appalachian Mountains (*64*). We calculated the actual vapor content of the air using:

$$e_a = \left(e^{\left[\left(\frac{1}{T_o} - \frac{1}{T_d}\right) \times \frac{L}{R_v}\right]} \times e_o \right) \quad (6)$$

where e_a is the actual vapor content, e_o = 0.611 kPa, T_o = 273 K, and R_v = 461.5 J K^{-1} kg^{-1} and L = 2.5x10^6 J/kg (latent heat of vaporization), and T_d is the minimum temperature at 600 that we assumed is the dew point temperature. We developed this equation based upon the Clausius-Clapeyron equation that is used to estimate saturation vapor pressure. We measured the saturation vapor pressure using the Clausius-Clapeyron equation:

$$e_s = e_o \cdot \exp\left[\frac{L}{R_v}\left(\frac{1}{T_o} - \frac{1}{T}\right)\right] \quad (7)$$

where e_o = 0.611 kPa and T_o = 273K are constant parameters, and R_v = 461.5 J K^{-1} kg^{-1} and L = 2.5x10^6 J/kg are the gas constant for water vapor and the latent heat of vaporization, respectively. The saturation vapor pressure then allowed us to calculate the vapor pressure deficit using:

$$VPD = e_s - e_a \quad (8)$$

where e_s is the saturation vapor pressure (kPa) at a given temperature and e_a is the vapor pressure of ambient air (kPa). To estimate VPDs in the future, we assumed that relative humidities remained the same during climate change, an emergent characteristic of

general circulation models (*22*). We estimated warming from the IPCC (2014) report on climate change using:

$$T_{RCP85} = (-0.555 \times year) + (1.454 \times 10^{-4} \times year^2) + 528.36 \quad (9)$$

where T_{RCP85} is the estimated increase in temperature at a given year. To generate the function, we used DataThief™ to produce statistical models of the RCP85 climate warming scenario.

Calculations for foraging-energetic species distribution model

The foraging-energetic model was built upon the estimation of body temperature and thermally-sensitive traits. Body temperatures were estimated using humid operative temperature (T_{eh}) to account for radiative balance at night and the loss of heat associated with evaporative cooling (*52*). We estimated T_{eh} using:

$$T_{eh} = T_a + \frac{\gamma^*}{s + \gamma^*}\left(\frac{R_{abs} - \varepsilon_s \sigma T_a^4}{c_p g_{Hr}} - \frac{D}{\gamma^* p_a}\right) \quad (10)$$

where T_a is ambient temperature, s is the slope of saturation mole fraction function, R_{abs} is the absorbed short- and long-wave radiation, γ^* is the apparent psychrometer constant, ε_s is the emissivity of the salamander (0.96), sigma is the Stefan-Boltzmann constant, c_p is the specific heat of air at constant pressure, g_{Hr} is the sum of boundary layer and radiative conductances, D is the vapor pressure deficit of the air, and p_a is the atmospheric air pressure. We estimated the thermal sensitivity of energy assimilated from prey using:

$$E_a = 0.003835 + (-0.002522) \times T + 0.0009089 \times \mathrm{T}^2 + (-2.527 \times 10^{-5}) \times T^3 \quad (11)$$

where E_a is energy assimilated from prey (kJ g^{-1} day^{-1}), and T is body temperature (°C) (*55*). The relationship is corrected for mass; therefore, the resulting value can be multiplied by the mass of the salamander to provide an estimate of foraging intake at a given body size. We used these daily rates of energy intake to calculate the energy intake for each minute that the salamander was active. By using these equations, we assume that salamanders immediately consume and digest their prey. We estimated energetic costs from $\dot{V}O_2$ using:

$$\dot{V}O_2 = (0.0416 \times T) + 0.386 \times \log(mass) \quad (12)$$

where $\dot{V}O_2$ is the volume of oxygen consumption (μL/min), T is temperature (°C), and *mass* is the mass (g) of the salamander. We assumed a mixed diet of fats and carbohydrates to estimate a respiratory quotient of 0.8 to calculate energetic costs in Joules from $\dot{V}O_2$ (*65*). We estimated energetic costs underground from soil temperatures at a given depth and time using:

$$T = T_{ave} + A(0)\exp(-z/D)\sin[\omega(t-8) - z/D] \quad (13)$$

where T_{ave} is the mean daily soil surface temperature, ω is $\pi/12$, $A(0)$ is the amplitude of the temperature fluctuations at the surface, D is the damping depth, and t is the time of day (hr) (*52*). We used 5.238 as the damping depth based upon empirically derived values for soil type and moisture for the southern Appalachians (*66*).

Predicting extinction

We estimated extinction based upon the depletion of lipid reserves at a given body size. Fat reserves typically constitute 25% of the dry mass of a plethodontid salamander and

are primarily triglycerides (*58*). With triglycerides containing 38 kJ per gram (*67*), we estimated the energy reserves using:

$$LR = (1.9855 \times mass) + 0.1663 \quad (14)$$

where LR is the lipid reserves (kJ) and *mass* is the mass (g) of the salamander in grams. Once an individual depleted their entire lipid reserves, we assumed the location could no longer support salamanders.

Statistical analyses

We conducted statistical analyses in *R* (v. 3.2.4) for all physiological experiments. We analyzed the variation in r_i and $\dot{V}O_2$ using a linear model with time point and elevation as factors and body size of the individual as a covariate. We then conducted a type II analysis of variance (ANCOVA) using the *car* package in *R* to assess independent effects of interactions. We plotted means adjusted for mass that we calculated using the *effects* package in *R*. We calculated omega-squared (ω^2) to determine the proportion of variation explained by each component while controlling for error and sample size. We calculated omega-squared (ω^2) using:

$$\omega^2 = \frac{SS_{treatment} - df_{treatment} \times MS_{error}}{SS_{total} + MS_{error}} \quad (15)$$

where $SS_{treatment}$ is the sum of squares for a given parameter, $df_{treatment}$ is the degrees of freedom for that parameter, MS_{error} is the mean square error, and SS_{total} is the total sum of squares (*68*). For the species distribution model, we used a similar approach to determine the proportion of variation that body size, skin resistance, and behavior influenced model predictions using a type II ANCOVA. The simulations had several levels of dehydration thresholds (3.5%, 7%,10%), with and without behavioral

avoidance, skin resistance to water loss (4 s/cm, 7 s/cm), and body size (2 g, 3 g, 4 g, 5 g) under the climate warming scenario (RCP85) with all possible combinations to assess sensitivity of extinction to model parameters. The model also accounted for the influence of warming by including year as a covariate. For the laboratory experiments, we wanted to demonstrate that individuals exhibited plasticity in the laboratory. We identified plasticity in r_i by determining the relationship between r_i and the change in r_i that occurred during the experiment. We used a type II ANCOVA to assess the relationship between initial r_i and change in r_i over the course of the experiment. All additional calculations for proportion of extinct regions in the model were calculated using custom code in Python.

Tables

Table S1. Analysis of covariance and effect sizes for seasonal acclimatization demonstrates that surface area and month have the greatest influence on skin resistance to water loss (r_i). The total samples size was 180 individuals with 36 individuals measured at each time point. Values in bold represent statistically significant effects.

predictor	**SS**	***df***	***F***	***p***	**ω^2**
surface area	128	1	240	**<0.001**	0.46
elevation	0.754	2	0.712	0.49	<0.01
time point	54.1	4	25.5	**<0.001**	0.19
surface area * elevation	0.565	2	0.533	0.58	<0.01
surface area * time point	3.32	4	1.57	0.18	<0.01
elevation * time point	3.13	8	0.739	0.65	<0.01
surface area * elevation * time point	3.36	8	0.788	0.61	<0.01
residuals	79.4	150			

SS = sum of squares, ω^2 = effect size

Table S2. Analysis of covariance and effect size for the seasonal acclimatization experiment demonstrates that surface area and month had the greatest effect on metabolic rate ($\dot{V}O_2$) during the summer. The total samples size was 180 individuals with 36 individuals measured at each time point. Bolded values are statistically significant.

predictor	**SS**	***df***	***F***	***p***	$\boldsymbol{\omega^2}$
mass	36576	1	15.1	**<0.001**	0.04
elevation	8242	2	1.69	0.18	0.02
time point	21956	4	2.26	0.06	0.04
mass * elevation	214	2	0.0441	0.95	<0.01
mass * time point	1013	4	0.104	0.98	<0.01
elevation * time point	2595	8	0.134	0.99	<0.01
mass * elevation * time point	6378	8	0.328	0.95	<0.01
residuals	364205	150			

SS = sum of squares, $\boldsymbol{\omega}^2$ = effect size

Table S3. Analysis of covariance and effect size on the simulated data from the mechanistic SDM illustrates that mass had the largest influence on the number of extinct regions in the species range model.

predictor	**SS**	***df***	***F***	***p***	$\boldsymbol{\omega^2}$
activity threshold	1.79×10^{12}	1	1090	<0.001	0.21
mass	2.19×10^{12}	1	1340	<0.001	0.53
avoidance behavior	6.43×10^{10}	1	39.3	<0.001	0.02
acclimatization	2.36×10^{11}	1	144	<0.001	0.07
year	3.85×10^{11}	1	235	<0.001	0.06
residuals	8.55×10^{11}	522			

SS = sum of squares, $\boldsymbol{\omega}^2$ = effect size

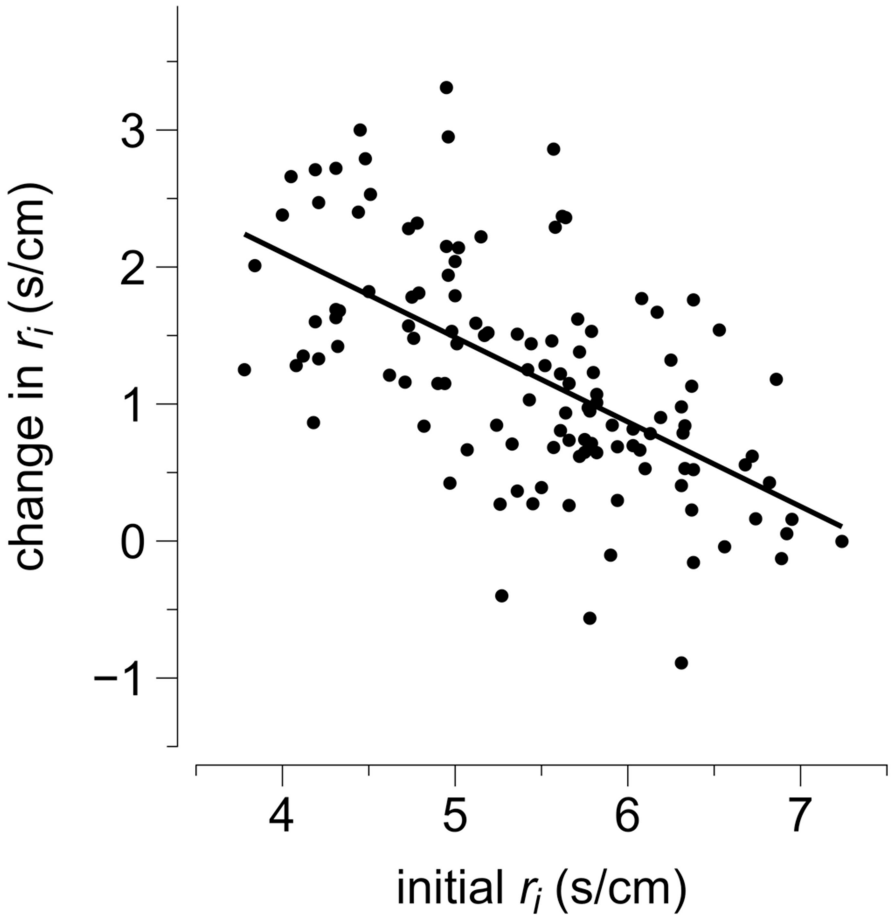

Fig. S1. Experimental evidence for physiological plasticity of skin resistance to water loss. Individuals with initially low values of r_i dramatically increased the resistance of their skin to water loss during the course of the experiment (p<0.001, r^2= 0.36). Moreover, individuals with high resistances tended to maintain the same r_i throughout the experiment. The pattern suggests that high r_i represents an important strategy for limiting the threat of dehydration during bouts of activity under controlled laboratory conditions. The purpose of the figure was to simply demonstrate that individuals exhibit plasticity of r_i.

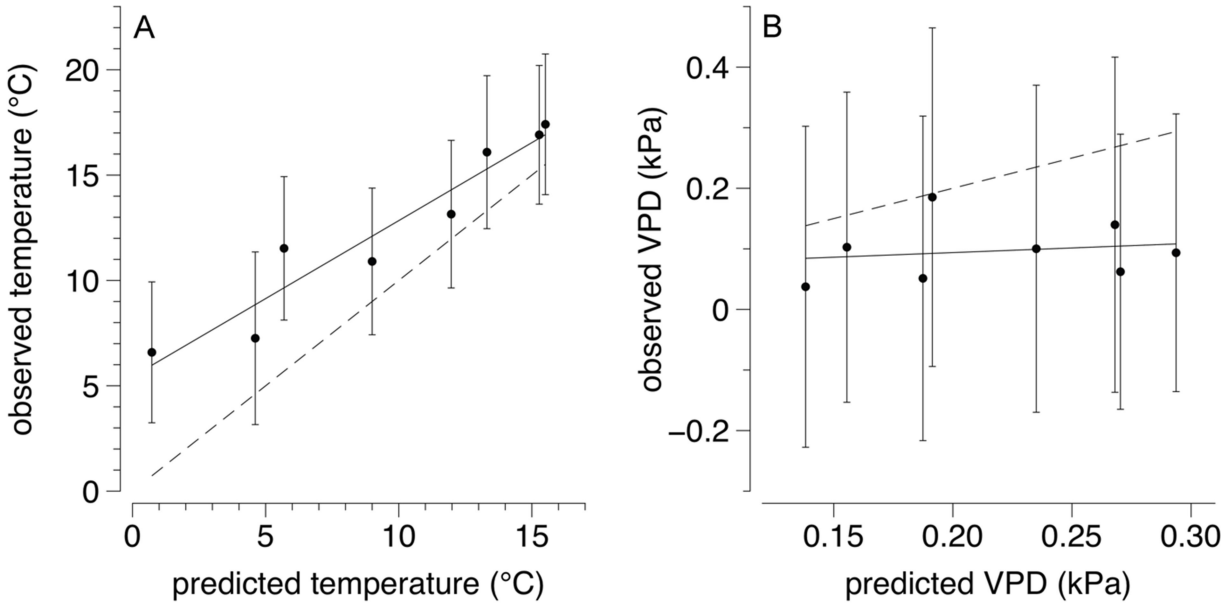

Fig. S2. Predicted and observed values of nighttime temperatures and VPDs at our field site near Cullowhee, NC. Predicted temperatures were generated from the *microclim* dataset, and predicted vapor pressure deficits (VPDs) were assumed from minimum temperatures. Solid lines represent regression between predicted and observed values, and the dotted lines represents the expected regression for a perfect fit between predicted and observed values. Our predicted estimates of VPD were drier than the observed values but fell within the variation experienced by terrestrial salamanders.

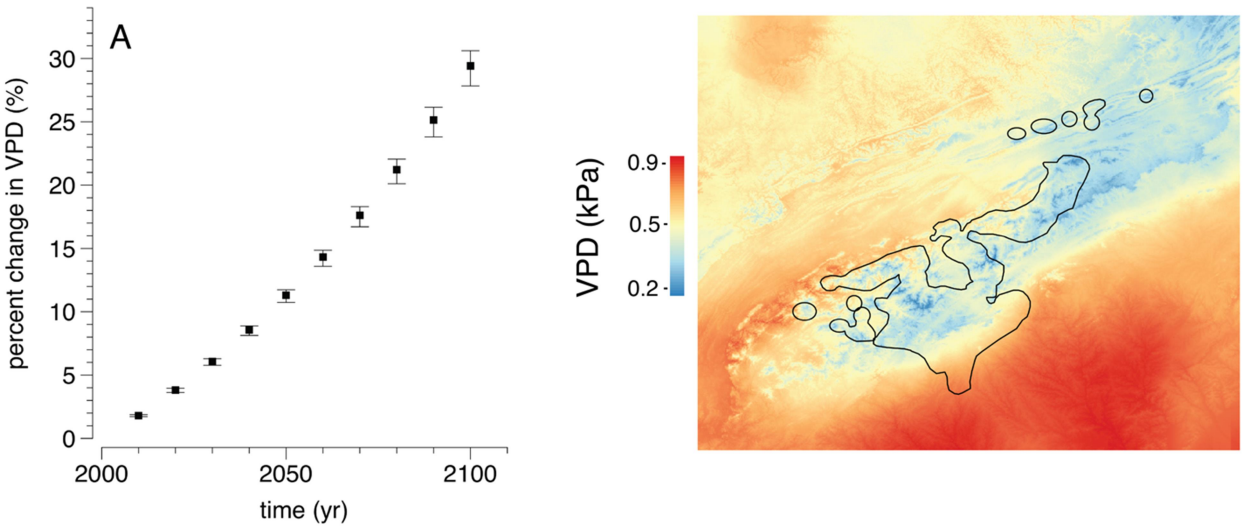

Fig. S3. Estimated rise in VPDs through time under climate change and the spatial distribution of VPDs in 2100. The figure demonstrates (A) the mean and range of percent rise in VPDs over the century every ten years in relation to the year 2000. The figure also illustrates (B) the spatial variation in VPDs across the southern Appalachian Mountains in relation to the current distribution of the *P. jordani* species complex. High elevations are predicted to exhibit the most saturated air averaged across the year.

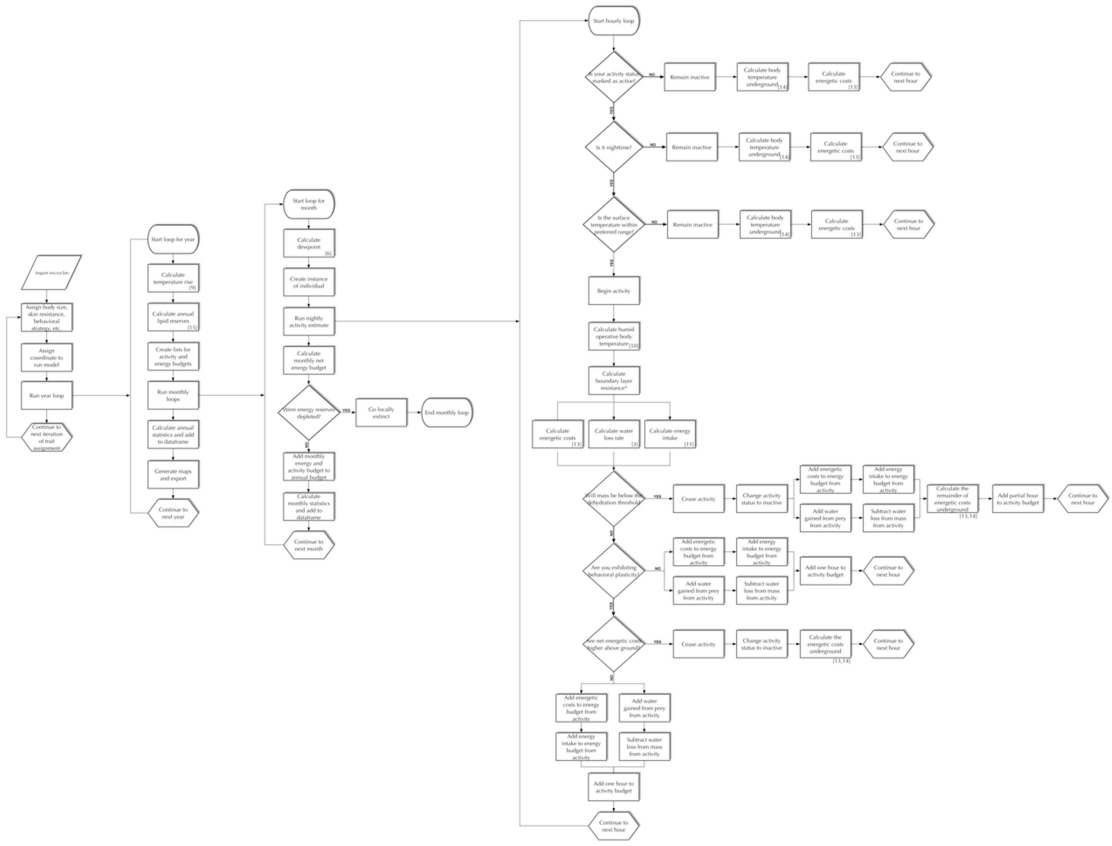

Fig. S4. Flow chart of foraging-energetic model used to estimate extinction. The design of the foraging-energetic model that describes the inputs (*microclim*), decisions (triangles), processes (rectangles), and loops (diamonds). The figure demonstrates that the model runs in an iterative manner with every combination of body size, skin resistance, dehydration threshold, and depth. We selected 10 yr intervals to run the model from contemporary climates to end of the century to demonstrate the changes in habitat suitability. We noted the calculations that were used for a particular process within or underneath the rectangle, if appropriate.